



ELSEVIER

Applied Numerical Mathematics 36 (2001) 155–178



APPLIED  
NUMERICAL  
MATHEMATICS

www.elsevier.nl/locate/apnum

# A comparison of classical and new finite element methods for the computation of laminate microstructure

Matthias K. Gobbert<sup>a,\*</sup>, Andreas Prohl<sup>b</sup>

<sup>a</sup> *Department of Mathematics and Statistics, University of Maryland, Baltimore County, 1000 Hilltop Circle, Baltimore, MD 21250, USA*

<sup>b</sup> *Mathematisches Seminar, Christian-Albrechts-Universität Kiel, Ludewig-Meyn-Str. 4, D-24098 Kiel, Germany*

---

## Abstract

A geometrically nonlinear continuum theory has been developed for the equilibria of martensitic crystals based on elastic energy minimization. For these non-convex functionals, typically no classical solutions exist, and minimizing sequences involving Young measures are studied. Direct minimizations using discretization based on conforming, non-conforming, and discontinuous elements have been proposed for the numerical approximation of this problem. Theoretical results predict the superiority of the discontinuous finite element. Detailed numerical studies of the available finite element discretizations in this paper validate the theory. One-dimensional prototype problems due to Bolza and Tartar and a two-dimensional numerical model of the Ericksen–James energy are presented. Both classical elements yield solutions that possess suboptimal convergence rates and depend heavily on the underlying numerical mesh. The discontinuous finite element method overcomes this problem and shows optimal convergence behavior independent of the numerical mesh. © 2001 IMACS. Published by Elsevier Science B.V. All rights reserved.

*Keywords:* Ericksen–James energy density; Finite element method; Non-convex minimization; Nonlinear conjugate gradients; Multi-well problem; Nonlinear elasticity; Materials science

---

## 1. Introduction

Many new materials of interest in materials science and structural mechanics have been found to exhibit microstructure under certain ambient conditions. For example, certain alloys show laminate microstructure that can be observed in laboratory experiments [1,2]. The understanding of these microscopic phenomena plays an important role to improve certain material properties like shape-memory, ferroelectricity, or magnetostriction, used for instance in micromachines.

---

\* Corresponding author.

*E-mail addresses:* gobbert@math.umbc.edu (M.K. Gobbert), apr@numerik.uni-kiel.de (A. Prohl).

A mathematical model for such ‘smart materials’ was first given by Ball and James [1,2]. In there, minimizing solutions represent deformations that exhibit microstructures which are observed in experiments. A particular example is the phenomenon of twinning associated with austenite-martensite transformations [1,2].

Because of the non-(quasi-)convex nature of the so-called Ericksen–James energy density, the related functional is not weakly lower semicontinuous and hence there is a lack of a minimizer belonging to an appropriate underlying Sobolev space, in general. Instead, corresponding (weakly converging) minimizing sequences are studied that typically show fast oscillations in the gradient of the deformation which gives rise to microstructure. A tool for describing the asymptotic behavior of minimizing sequences is the Young measure [23], giving volume fractions of the involved martensitic variants in each test volume of the reference domain in austenite state  $\Omega$ . This probability measure enables the evaluation of (nonlinear) quantities, like the stress for the limit of such minimizing sequences [23].

From the numerical point of view, the computation of minimizers associated with discrete models leads to significant problems, mainly caused by their non-convex character. Over the last years, basically three categories of methods have been studied to cope with this type of problem:

1. *Convexification of the energy functional*, see, e.g., [4,10,14,23]: The original non-convex elastic energy density is replaced by its (quasi- or rank-one-)convex hull. This manipulation is attractive since now a minimizer exists that is the weak limit of a minimizing sequence. Equally important, the solution of this problem is now accessible to standard gradient based minimization routines. On the other hand, explicit formulae of (quasi-)convex hulls are only known in some cases (unfortunately, the physically important case of the Ericksen–James energy functional is not covered), and numerical approximations of it are rather expensive, see [4]. Moreover, this process deletes physical information from the original energy functional that makes this approach questionable for certain important applications.
2. *Generalized formulation of the energy functional*, see, e.g., [6,23,24]: The original problem is reformulated as a convex minimization problem in terms of the deformation and parameterized gradient Young measures. This approach is quite promising from a theoretical point of view since the energy functional is kept unchanged. As a drawback, it causes significant computational work which necessitates additional sophisticated numerical strategies. A first promising step to reduce computational work is given in [6], where a one-dimensional test problem is studied.
3. *Direct minimization of the energy functional*, see, e.g., [8,11,16,15,18–21]: Numerical methods that fit into this category start with discretizations of the energy functional and underlying domain via, e.g., finite element methods. These methods preserve the physical energy density and are applicable without restrictions. On the other hand, they might suffer severely from the non-convex character of the energy density in that computed minimizers often get stuck in local minima. Furthermore, the spatial discretization introduces a scaling to the microstructure that limits the resolution of complex microstructure. At the same time, this drawback of local minima is sometimes advantageous for applications where local minima (e.g., “metastable states”) are important (e.g., in hysteresis phenomena).

In the following, we consider finite element methods that are intended for the direct minimization of non-convex functionals. In the context of the Ericksen–James energy density, we refer to the extensive survey article by Luskin [19] and the publications [15,16,18,21] that deal with the numerical analysis of conforming and classical non-conforming methods (i.e., continuity is only enforced in the center of adjacent finite element faces). As is pointed out in these contributions, the resolution of microscale

structures heavily relies on the alignment of the underlying mesh with the laminated microstructure, otherwise leading to drastically polluted solutions.

This is the basic motivation for the introduction of discontinuous finite element methods to this type of minimization problem. As can be clearly seen from the theoretical investigations performed in [11], the convergence analysis leads to results that are superior to those of conforming and classical non-conforming methods, which reflects the increased flexibility of the finite element method with respect to the underlying triangulation.

Mathematical models for describing deformations from a reference state of ‘smart materials’ can be formulated in two or three dimensions, i.e.,  $d \in \{2, 3\}$ . The numerical problem reads then as follows. For the reference state  $\Omega \in \mathbb{R}^d$ , minimize the energy functional

$$\mathcal{E}(v) = \int_{\Omega} \phi(\nabla v(x)) \, dx \quad (1)$$

over all admissible functions  $v \in \mathcal{A}$  with

$$\mathcal{A} = \{u \in C(\bar{\Omega}; \mathbb{R}^d) : u|_{\partial\Omega} = g(x)\}. \quad (2)$$

Here,  $\phi: \mathbb{R}^{d \times d} \rightarrow \mathbb{R}$  is the Ericksen–James energy, that only depends on the gradient  $\nabla v$  of the deformation  $v$ , and  $g(x)$  is a given function on the boundary of  $\Omega$ . The Ericksen–James energy density satisfies the principle of frame indifference and leads to a non-convex energy functional to be minimized. For a detailed discussion on the physical background of the energy, we refer to [19]. For the subsequent studies, we benefit from the density  $\phi(\cdot)$  being non-negative and  $\phi(A) = 0$  if and only if  $A \in \mathcal{U}$ , where  $\mathcal{U}$  denotes the union of all energy wells. These wells correspond to symmetry-related energy-minimizing states of the material.

In order to have minimizers being Lipschitz-continuous, the wells have to be rank-one connected. For the case of a two-well problem, this implies the condition

$$\exists F_i \in \mathcal{U}_i, \quad i = 1, 2, \quad \exists a, n \in \mathbb{R}^3 \quad \text{such that} \quad F_2 = F_1 + a \otimes n.$$

Here,  $\otimes$  denotes the tensor product of the vectors  $a$  and  $n$ , that is,  $(a \otimes n)_{ij} = a_i n_j$ . Without loss of generality, we may assume  $|n| = 1$ . To guarantee uniqueness of a homogeneous gradient Young measure that is associated with this microstructure [1,2], we prescribe affine boundary conditions

$$u(x) = F_{\lambda} x \quad \text{for } x \in \partial\Omega, \quad (3)$$

where

$$F_{\lambda} = \lambda F_1 + (1 - \lambda) F_2 \quad (4)$$

with volume fraction  $\lambda \in [0, 1]$ . These characterizations of admissible deformations generalize to the multi-well case of several energetically equivalent crystallographic configurations, see, e.g., [19].

The first finite element methods for the minimization of (1) used conforming elements with piecewise linear basis functions on each triangular or quadrilateral element, thus minimizing on a set of admissible functions  $\mathcal{A}_h \subset \mathcal{A}$ . For strictly *convex* energy densities  $\phi$  and sufficiently smooth data, this approach is known to yield optimal convergence results for the energy with order  $O(h^2)$ . However, for the problem with a non-convex energy density, it can only be shown in general that a minimizing deformation  $u_h \in \mathcal{A}_h$  satisfies

$$\mathcal{E}(u_h) \leq Ch^{1/2}, \quad (5)$$

where the constant  $C$  may depend on the coefficients of the problem, the triangulation  $\mathcal{T}_h$  and the domain  $\Omega$ , but not on the mesh parameter  $h$ , see [7,8,15,18–20]. It has been observed that the quality of the approximation depends strongly on the degree of alignment of the numerical mesh with the physical laminates [9,19,21]. This means that the laminate microstructure is well-resolved on meshes, whose element edges run along the laminate direction. If this is not the case, the numerical results are often significantly polluted so that the laminates are distorted or, worse yet, align themselves with the numerical grid irrespective of the underlying physics [9,21].

As a second numerical approach, a classical non-conforming finite element method with continuity only in the edge midpoints (the Crouzeix–Raviart element) has been used [9,12,19,20]; even more general three dimensional non-conforming elements have been used in [13] and analyzed in [16]. This method relaxes the continuity constraints between each two elements by only requiring continuity of the discrete deformations at the edge midpoints. Of course, the functional  $\mathcal{E}(\cdot)$  is then defined in an appropriate element-wise setting by taking  $\mathcal{E}_h(\cdot)$ . This finite element method does have increased flexibility to handle deformations with microstructure on general grids due to the relaxation of the inter-element continuity requirements. However, the theoretical analysis presented in [12,16] does not reflect this improved flexibility in comparison to the conforming method, and the result for a minimizer  $u_h \in \mathcal{A}_h$  is still

$$\mathcal{E}_h(u_h) \leq Ch^{1/2}. \quad (6)$$

This motivates the construction of a new finite element method yielding more accurate approximations of crucial quantities such as the macroscopic deformation, the structure of laminates, and the statistical properties of the microstructure given in terms of its Young measure on general meshes. Moreover, this new method should be able to represent more complex microstructure given through force-driven deformations as well as ones occurring in evolutionary models both in this context and for more complicated materials.

An algorithm based on discontinuous finite elements was introduced in [11]. As it is shown there, this algorithm allows for much improved convergence rate estimates for the energy (namely,  $O(h^2)$  for the energy of a minimizing deformation) as well as other quantities of interest like the gradient Young measure or the deformation gradient in laminate direction. In particular, this result holds for non-aligned meshes, i.e., those that are independent of the alignment of the numerical grid with the physical laminates. The underlying conceptual ideas are the following:

1. The (averaged) boundary conditions will be treated in a more relaxed way to avoid the pollution impact from the boundary.
2. The cross-element continuity constraints are relaxed in the sense that small jumps are allowed.
3. The laminate structures are scaled differently from the transitions between laminates.

This leads to the following algorithm:

**Algorithm 1.** Given a quasiuniform triangulation  $\mathcal{T}_h$  of the domain  $\Omega \subset \mathbb{R}^d$ , with  $d \in \{2, 3\}$ , consider element-wise linear deformations  $v_h \in \mathcal{A}_h \equiv \prod_{K \in \mathcal{T}_h} \mathcal{P}_1(K)$  with the scaled energy functional

$$\begin{aligned} \mathcal{E}_h^\beta(v_h) = & \sum_{K \in \mathcal{T}_h} \int_K \phi(\nabla v_h(x)) \, dx + \alpha_{11} \left( \sum_{K \in \mathcal{T}_h} h^{1-\beta} \int_{\partial K} |[v_h](x)| \, d\sigma \right)^2 \\ & + \alpha_{12} \left( \sum_{K \in \mathcal{T}_h} h^{1-\beta} \int_{\partial K} |[v_h](x)|^2 \, d\sigma \right) + \alpha_2 \sum_{K \in \mathcal{T}_h} h^{2\beta} \int_{\partial K \cap \partial \Omega} |v_h(x) - F_\lambda x|^2 \, d\sigma, \end{aligned} \quad (7)$$

and perform the minimization

$$\min_{v_h \in \mathcal{A}_h} \mathcal{E}_h^\beta(v_h) \tag{8}$$

for a fixed constant  $\beta \in [0, 1]$ .

The coefficients  $\alpha_{11}$ ,  $\alpha_{12}$ , and  $\alpha_2$  are order one constants that control the relative contributions from the inter-element continuity constraints, and the relaxation of the boundary condition. Algorithm 1 introduces a different scaling of the physical information (i.e., the laminates, which are of order  $O(h^{1-\beta})$ ) and numerical scaling (i.e., transitions between laminates (of order  $O(h)$ )).

For the discontinuous element method, an energy estimate of  $O(h^2)$  holds [11]. This is optimal for the linear basis functions in use. However, this energy does not have a true physical meaning, but other quantities important for practical purposes are the following: The volume fractions  $\mu(\omega_\rho^i(u_h))/\mu(\omega)$  give approximations to the  $\lambda^i$ ,  $i \in \{1, 2\}$ , with  $\mu(\omega)$  the measure of the subdomain  $\omega$  and  $\mu(\omega_\rho^i(u_h))$  the measure of that collection of elements  $\omega_\rho^i \subset \omega$ , on which the deformation gradient  $\nabla u_h$  is inside a ball with radius  $\rho$  and center  $F_i$  (measured in the Frobenius norm). These quantities are crucial parameters in the computation of the gradient Young measure generated by the deformation gradient  $\nabla u_h$  [4]. The gradient Young measure in turn yields important macroscopic quantities of practical relevance, for instance, the stress field, see [4,19] and the literature cited therein. It is for this reason that the accurate approximation also of microscopic quantities like the deformation gradient and volume fraction is of importance. We recall here the main theorem that is proved in [11].

**Theorem 1.** Consider problem (8), with  $\beta = \frac{1}{2}$ , as an approximation of the minimization problem (1)–(2) with  $\Omega \subset \mathbb{R}^3$  a bounded set, and suppose  $u \in \mathcal{A}$  is a (weak limit) solution of problem (1)–(2) yielding zero energy with associated gradient Young measure  $\nu_x = \lambda^1 \delta_{F_1} + \lambda^2 \delta_{F_2}$ , where  $\nabla u(x) = \int_{\mathbb{R}^{d \times d}} A \, d\nu_x(A)$ . Then problem (8) has at least one solution  $u_h \in \mathcal{A}_h \equiv \prod_{K \in \mathcal{T}_h} \mathcal{P}_1(K)$ , and  $u_h$  satisfies the following convergence estimates, for all  $\omega \subset \Omega$  and  $h < \rho < 1$ , and all  $\rho > 0$ , for positive constants  $\alpha_{11}$ ,  $\alpha_{12}$  and  $\alpha_2$  of order one:

- (a)  $\mathcal{E}_h^{1/2}(u_h) \leq Ch^2$ ,
- (b)  $\|u_h - F_\lambda x\|_{L^2(\Omega)} \leq Ch^{1/4}$ ,
- (c)  $\|(\nabla u_h - F_\lambda)w\|_{L^2(\Omega)} \leq Ch^{1/4}$ ,
- (d)  $|\mu(\omega_\rho^i(u_h))/\mu(\omega) - \lambda^i| \leq Ch^{1/8}$ , for  $i \in \{1, 2\}$ .

The generic constant  $C$  may depend on the parameters of the continuous minimization problem, with energy (1) and the values  $\alpha_{11}$ ,  $\alpha_{12}$  and  $\alpha_2$ , but not on the mesh parameter  $h$ . In the case (d), it additionally depends on the choice of  $\rho$ .

The analytic convergence results for all quantities of interest and the different finite element methods that are subject to computational comparison in the following are summarized in Table 1. Here,  $\|\cdot\|$  stands for the  $L^2$ -norm. Moreover, the constants  $\lambda^i$ ,  $i \in \{1, 2\}$ , denote the coefficients of the gradient Young measure that are approximated by the volume fraction  $\mu(\omega_\rho^i(u_h))/\mu(\omega)$ ; for the double well problem, this is concretely  $\lambda^1 = \lambda$  and  $\lambda^2 = 1 - \lambda$ . A marked improvement over the classical methods can be observed for all quantities.

The purpose of this paper is a practical comparison of these different finite element methods for the direct minimization of the non-convex energy for several relevant energy densities. Specifically, a detailed

Table 1

Summary of convergence results for the energy and other crucial quantities for different finite element methods

Finite element method	$\mathcal{E}_h(u_h)$	$\ u_h - F_\lambda x\ $	$\ (\nabla u_h - F_\lambda) w\ $	$\left  \frac{\mu(\omega_p^j(u_h))}{\mu(\omega)} - \lambda^i \right $
Conforming [18,19]	$O(h^{1/2})$	$O(h^{1/8})$	$O(h^{1/8})$	$O(h^{1/16})$
Classical non-conforming [16]	$O(h^{1/2})$	$O(h^{1/8})$	$O(h^{1/8})$	$O(h^{1/16})$
Discontinuous [11]	$O(h^2)$	$O(h^{1/4})$	$O(h^{1/4})$	$O(h^{1/8})$

numerical case study for a one-dimensional prototype problem for simple laminates is presented in Section 2. This problem was originally proposed by Bolza, see, e.g., [23]. The results for the conforming element depend substantially on the alignment of the numerical grid with the physical laminates, while the non-conforming and discontinuous element are able to follow the laminates in all cases. However, both classical elements show substantially worse convergence rates than the discontinuous element. These results demonstrate the validity of the theoretical results contained in Table 1. A proposed modification of relaxing the enforcement of the boundary conditions also for the classical finite elements is shown to be ineffective in improving convergence rates in general. This demonstrates that the improvements gained for the discontinuous element are a result of the behavior in the interior of the domain.

Section 3 is devoted to the study of a more complex one-dimensional example due to Tartar. Its solution possesses microstructure only in part of the domain. Hence, this is a test of the flexibility of the methods to handle a more complex case than the one of simple laminates. The methods each exhibit the same behavior as for the simpler prototype problem, with the classical element suffering from numerical pollution in the case of non-aligned grids, while the discontinuous element is able to represent the physical situation adequately.

A classical two-dimensional model for orthorhombic to monoclinic transformations is studied in Section 4. This transformation is the physical example of two-well energy densities. The energy density following [19] exhibits all relevant features of the three-dimensional Ericksen–James energy and is used in many numerical studies of simple laminates, see [19]. Also in this case, the discontinuous element is able to represent the physics appropriately, while the conforming element suffers severe pollution of its results from the mis-alignment.

## 2. Example 1: A prototype problem for simple laminates

We consider the following prototype problem for the Ericksen–James energy [4,10]:

$$\mathcal{E}(v) = \int_{\Omega} ((v_x)^2 - 1)^2 + (v_y)^2 dx \quad (9)$$

for the domain  $\Omega = (0, 1) \times (0, 1) \subset \mathbb{R}^2$  and the deformations  $v: \Omega \rightarrow \mathbb{R}$  with boundary condition  $v = 0$  on  $\partial\Omega$ . The solution to this problem consists of laminates in the  $y$ -direction, because the favored deformation gradients  $\nabla v = (v_x, v_y)$  are  $F_1 = (+1, 0)$  and  $F_2 = (-1, 0)$ .

In order to study the dependence of the finite element method on the alignment of the numerical mesh with the physical laminates, we introduce the following generalized energy functional:

$$\mathcal{E}(v) = \int_{\Omega} ((\nabla v \cdot n)^2 - 1)^2 + (\nabla v \cdot w)^2 \, dx. \tag{10}$$

Here,  $n = n(\gamma) = (\cos(\gamma), \sin(\gamma))^T$  denotes the vector normal to the laminate direction,  $w = w(\gamma) \in \mathbb{R}^2$  is a vector along the laminates and orthogonal to  $n$ , and  $\gamma$  the angle between the positive  $x$ -axis and the vector  $n$ . Since the prototype problem with boundary condition  $u = 0$  on  $\partial\Omega$  models the example of simple laminates, the coefficients of the gradient Young measure  $\lambda^1$  and  $\lambda^2$  have to equal  $\frac{1}{2}$  in all cases.

We start with our comparison of the conforming, classical non-conforming, and discontinuous finite elements for this problem, by taking

$$\mathcal{E}_h^0(v_h) = \sum_{K \in \mathcal{T}_h} \int_K \phi(\nabla v_h(x)) \, dx + \alpha_2 \sum_{K \in \mathcal{T}_h} \int_{\partial K \cap \partial\Omega} |v_h(x) - F_\lambda x|^2 \, d\sigma \tag{11}$$

for both the conforming and the classical non-conforming method to study the impact of (averaged) boundary conditions in these schemes. For the discontinuous element, we choose the optimal coefficient  $\beta = \frac{1}{2}$  [11] and parameters  $\alpha_{11} = \alpha_{12} = \alpha_2 = 1$ . The angle  $\gamma$  is varied through five values to cover different mesh effects,  $\gamma \in \{-45^\circ, -22.5^\circ, 0^\circ, +22.5^\circ, +45^\circ\}$ . The mesh is given by a regularly refined triangular mesh independent of the angle  $\gamma$  and such that the mesh is fully aligned with the physical laminates when  $\gamma = -45^\circ$  and  $\gamma = 0^\circ$ . A study for the parameter  $\alpha_2$  governing the degree of relaxation of the boundary term was performed for the classical element by choosing either  $\alpha_2 = 1000$  for strict enforcement of the boundary conditions or  $\alpha_2 = 1$  for relaxed enforcement.

The computer program implements the nonlinear conjugate gradient method for the minimization with a quadratic fit line search after bracketing [17]. The energy functional of Algorithm 1 is discretized using the package FEAT2D [3] for the underlying finite element discretization. New element routines were defined in this package for the discontinuous finite element for our purposes.

### 2.1. The conforming finite element

This element has been considered computationally by Collins, see [8,9], and the convergence analyses are contained in [7,15,18,19]. Fig. 1 shows the computed volume fraction of the laminate microstructure. If the numerical mesh is well aligned with the physical laminates, the element represents the physical situation well. However, if the alignment is not good, distortion is possible (Fig. 1(d)), or the laminates grow wider than expected (Fig. 1(e)).

Table 2(a) lists the values of the computed energy functional for the conforming finite element. Note that for  $\gamma = -45^\circ$  and  $\gamma = 0^\circ$  the convergence rate is linear, due to the mesh being aligned with the direction of the physical laminates. In the other cases, however, the convergence rate is observed to be much less than  $O(h)$ .

Tables 3(a), 4(a), and 5(a) show the numerical results for the quantities listed in columns 2, 3, and 4 of Table 1. For the  $L^2$ -error of the deformation in Table 3(a), we observe nearly linear convergence for all angles  $\gamma$ , which is significantly better than the theoretically predicted rate of  $O(h^{1/8})$ , see Table 1. However, the  $L^2$ -error of the deformation gradient in laminate direction in Table 4(a) as well as the approximation to the volume fraction in Table 5(a) depend crucially on the alignment of the numerical mesh.

Table 2  
Total energy (column 1 in Table 1)

	$\gamma = -45^\circ$	$\gamma = -22.5^\circ$	$\gamma = 0^\circ$	$\gamma = +22.5^\circ$	$\gamma = +45^\circ$
(a) for the conforming element with $\alpha_2 = 1000$					
$h = \frac{1}{4}$	0.5754	0.5305	0.4532	0.6690	0.8920
$h = \frac{1}{8}$	0.3497	0.3604	0.3891	0.4617	0.6182
$h = \frac{1}{16}$	0.1884	0.2634	0.1939	0.3444	0.4260
$h = \frac{1}{32}$	0.0972	0.1958	0.0963	0.2512	0.2911
$h = \frac{1}{64}$	0.0488	0.1587	0.0474	0.1956	0.2320
(b) for the conforming element with $\alpha_2 = 1$					
$h = \frac{1}{4}$	0.1703	0.2791	0.1145	0.2460	0.5335
$h = \frac{1}{8}$	0.0435	0.1563	0.0425	0.2510	0.3300
$h = \frac{1}{16}$	0.0113	0.1251	0.0112	0.1676	0.3227
$h = \frac{1}{32}$	0.0029	0.1180	0.0029	0.1659	0.3459
$h = \frac{1}{64}$	0.0007	0.1162	0.0007	0.1861	0.3758
(c) for the classical non-conforming element with $\alpha_2 = 1000$					
$h = \frac{1}{4}$	0.2297	0.2629	0.3733	0.3833	0.3265
$h = \frac{1}{8}$	0.1532	0.1744	0.1996	0.2315	0.2200
$h = \frac{1}{16}$	0.0885	0.0980	0.0992	0.1438	0.1507
$h = \frac{1}{32}$	0.0470	0.0652	0.0491	0.0960	0.1085
$h = \frac{1}{64}$	0.0238	0.0392	0.0243	0.0765	0.0679
(d) for the classical non-conforming element with $\alpha_2 = 1$					
$h = \frac{1}{4}$	0.1422	0.1982	0.0880	0.2305	0.0938
$h = \frac{1}{8}$	0.0356	0.0612	0.0347	0.0957	0.0678
$h = \frac{1}{16}$	0.0093	0.0271	0.0092	0.0631	0.0132
$h = \frac{1}{32}$	0.0024	0.0171	0.0024	0.0524	0.0033
$h = \frac{1}{64}$	0.0006	0.0145	0.0006	0.0520	0.0115
(e) for the discontinuous element					
$h = \frac{1}{4}$	0.0165	0.0521	0.0173	0.0849	0.1156
$h = \frac{1}{8}$	0.0052	0.0222	0.0047	0.0324	0.0481
$h = \frac{1}{16}$	0.0007	0.0052	0.0007	0.0108	0.0192
$h = \frac{1}{32}$	0.0005	0.0014	0.0007	0.0033	0.0038
$h = \frac{1}{64}$	0.0000	0.0003	0.0000	0.0009	0.0013

Table 3  
Error of the deformation in the  $L^2$ -norm (column 2 in Table 1)

	$\gamma = -45^\circ$	$\gamma = -22.5^\circ$	$\gamma = 0^\circ$	$\gamma = +22.5^\circ$	$\gamma = +45^\circ$
(a) for the conforming element with $\alpha_2 = 1000$					
$h = \frac{1}{4}$	0.0733	0.0890	0.0980	0.1068	0.0800
$h = \frac{1}{8}$	0.0773	0.0832	0.1171	0.0904	0.1043
$h = \frac{1}{16}$	0.0459	0.0574	0.0658	0.0685	0.0857
$h = \frac{1}{32}$	0.0243	0.0309	0.0345	0.0452	0.0648
$h = \frac{1}{64}$	0.0125	0.0158	0.0177	0.0274	0.0308
(b) for the conforming element with $\alpha_2 = 1$					
$h = \frac{1}{4}$	0.1882	0.1997	0.1897	0.1838	0.1975
$h = \frac{1}{8}$	0.1004	0.1433	0.1398	0.1363	0.1208
$h = \frac{1}{16}$	0.0509	0.0653	0.0717	0.0855	0.0590
$h = \frac{1}{32}$	0.0255	0.0325	0.0360	0.0441	0.0276
$h = \frac{1}{64}$	0.0128	0.0162	0.0180	0.0185	0.0122
(c) for the classical non-conforming element with $\alpha_2 = 1000$					
$h = \frac{1}{4}$	0.1055	0.1332	0.1708	0.1405	0.1194
$h = \frac{1}{8}$	0.0857	0.0954	0.1196	0.0957	0.0765
$h = \frac{1}{16}$	0.0473	0.0586	0.0662	0.0585	0.0424
$h = \frac{1}{32}$	0.0246	0.0315	0.0346	0.0313	0.0241
$h = \frac{1}{64}$	0.0125	0.0162	0.0177	0.0163	0.0125
(d) for the classical non-conforming element with $\alpha_2 = 1$					
$h = \frac{1}{4}$	0.1864	0.2194	0.1991	0.1980	0.1536
$h = \frac{1}{8}$	0.1003	0.1468	0.1396	0.1452	0.1137
$h = \frac{1}{16}$	0.0509	0.0664	0.0716	0.0670	0.0592
$h = \frac{1}{32}$	0.0255	0.0334	0.0360	0.0337	0.0289
$h = \frac{1}{64}$	0.0128	0.0167	0.0180	0.0168	0.0135
(e) for the discontinuous element					
$h = \frac{1}{4}$	0.0960	0.1223	0.1375	0.1301	0.1233
$h = \frac{1}{8}$	0.0673	0.0915	0.1015	0.0896	0.0728
$h = \frac{1}{16}$	0.0505	0.0658	0.0718	0.0634	0.0519
$h = \frac{1}{32}$	0.0351	0.0468	0.0504	0.0458	0.0357
$h = \frac{1}{64}$	0.0255	0.0332	0.0361	0.0327	0.0251

Table 4

Error of the deformation gradient in laminate direction in the  $L^2$ -norm (column 3 in Table 1)

	$\gamma = -45^\circ$	$\gamma = -22.5^\circ$	$\gamma = 0^\circ$	$\gamma = +22.5^\circ$	$\gamma = +45^\circ$
(a) for the conforming element with $\alpha_2 = 1000$					
$h = \frac{1}{4}$	0.2665	0.3946	0.4089	0.5459	0.4849
$h = \frac{1}{8}$	0.3135	0.3942	0.4368	0.4842	0.5063
$h = \frac{1}{16}$	0.2474	0.3297	0.3086	0.4135	0.4483
$h = \frac{1}{32}$	0.1834	0.2758	0.2158	0.3446	0.3805
$h = \frac{1}{64}$	0.1313	0.2330	0.1496	0.3145	0.3255
(b) for the conforming element with $\alpha_2 = 1$					
$h = \frac{1}{4}$	0.0173	0.2006	0.0653	0.3002	0.3375
$h = \frac{1}{8}$	0.0199	0.1975	0.0398	0.2741	0.3216
$h = \frac{1}{16}$	0.0105	0.1882	0.0137	0.2302	0.3502
$h = \frac{1}{32}$	0.0037	0.1872	0.0045	0.2324	0.3670
$h = \frac{1}{64}$	0.0013	0.1880	0.0015	0.2477	0.3886
(c) for the classical non-conforming element with $\alpha_2 = 1000$					
$h = \frac{1}{4}$	0.3547	0.4289	0.5002	0.4291	0.2750
$h = \frac{1}{8}$	0.3427	0.3598	0.4017	0.3486	0.2356
$h = \frac{1}{16}$	0.2657	0.2778	0.2813	0.2839	0.2018
$h = \frac{1}{32}$	0.1945	0.2221	0.1978	0.2313	0.1994
$h = \frac{1}{64}$	0.1374	0.1690	0.1373	0.1965	0.1551
(d) for the classical non-conforming element with $\alpha_2 = 1$					
$h = \frac{1}{4}$	0.0419	0.1461	0.0884	0.1922	0.0368
$h = \frac{1}{8}$	0.0358	0.0982	0.0519	0.1502	0.1573
$h = \frac{1}{16}$	0.0167	0.0883	0.0194	0.1495	0.0137
$h = \frac{1}{32}$	0.0063	0.0950	0.0068	0.1509	0.0051
$h = \frac{1}{64}$	0.0023	0.0961	0.0023	0.1525	0.0630
(e) for the discontinuous element					
$h = \frac{1}{4}$	0.0097	0.0772	0.0169	0.0635	0.0897
$h = \frac{1}{8}$	0.0058	0.0484	0.0062	0.0374	0.0471
$h = \frac{1}{16}$	0.0012	0.0142	0.0011	0.0164	0.0185
$h = \frac{1}{32}$	0.0008	0.0047	0.0007	0.0063	0.0056
$h = \frac{1}{64}$	0.0002	0.0015	0.0001	0.0021	0.0020

Table 5

Error in the volume fraction  $\lambda^1$  for  $\omega = \Omega$  (column 4 in Table 1 with  $i = 1$ )

	$\gamma = -45^\circ$	$\gamma = -22.5^\circ$	$\gamma = 0^\circ$	$\gamma = +22.5^\circ$	$\gamma = +45^\circ$
(a) for the conforming element with $\alpha_2 = 1000$					
$h = \frac{1}{4}$	0.3125	0.3750	0.2500	0.4375	0.5000
$h = \frac{1}{8}$	0.1875	0.2344	0.2500	0.2578	0.3125
$h = \frac{1}{16}$	0.1172	0.1816	0.1250	0.1816	0.2188
$h = \frac{1}{32}$	0.0645	0.1704	0.0625	0.1455	0.1533
$h = \frac{1}{64}$	0.0337	0.1477	0.0303	0.1028	0.1326
(b) for the conforming element with $\alpha_2 = 1$					
$h = \frac{1}{4}$	0.2500	0.1562	0.0000	0.1562	0.5000
$h = \frac{1}{8}$	0.0000	0.1484	0.0000	0.1328	0.1562
$h = \frac{1}{16}$	0.0000	0.1074	0.0000	0.0703	0.1797
$h = \frac{1}{32}$	0.0000	0.1191	0.0000	0.1055	0.2168
$h = \frac{1}{64}$	0.0000	0.1234	0.0000	0.1218	0.2324
(c) for the classical non-conforming element with $h = \alpha_2 = 1000$					
$h = \frac{1}{4}$	0.3125	0.1875	0.2500	0.3438	0.2500
$h = \frac{1}{8}$	0.0469	0.0859	0.1250	0.2344	0.2031
$h = \frac{1}{16}$	0.0586	0.0703	0.0625	0.1504	0.2109
$h = \frac{1}{32}$	0.0381	0.0527	0.0312	0.1216	0.1641
$h = \frac{1}{64}$	0.0212	0.0326	0.0154	0.1105	0.1029
(d) for the classical non-conforming element with $\alpha_2 = 1$					
$h = \frac{1}{4}$	0.2500	0.0312	0.0000	0.2188	0.1250
$h = \frac{1}{8}$	0.0000	0.0078	0.0000	0.0781	0.0156
$h = \frac{1}{16}$	0.0000	0.0000	0.0000	0.0762	0.0312
$h = \frac{1}{32}$	0.0000	0.0137	0.0000	0.0869	0.0156
$h = \frac{1}{64}$	0.0000	0.0144	0.0000	0.0902	0.0134
(e) for the discontinuous element					
$h = \frac{1}{4}$	0.0000	0.0000	0.0000	0.0000	0.0625
$h = \frac{1}{8}$	0.0312	0.0547	0.0000	0.0781	0.0312
$h = \frac{1}{16}$	0.0000	0.0000	0.0000	0.0000	0.0020
$h = \frac{1}{32}$	0.0186	0.0029	0.0312	0.0049	0.0068
$h = \frac{1}{64}$	0.0000	0.0000	0.0000	0.0000	0.0000

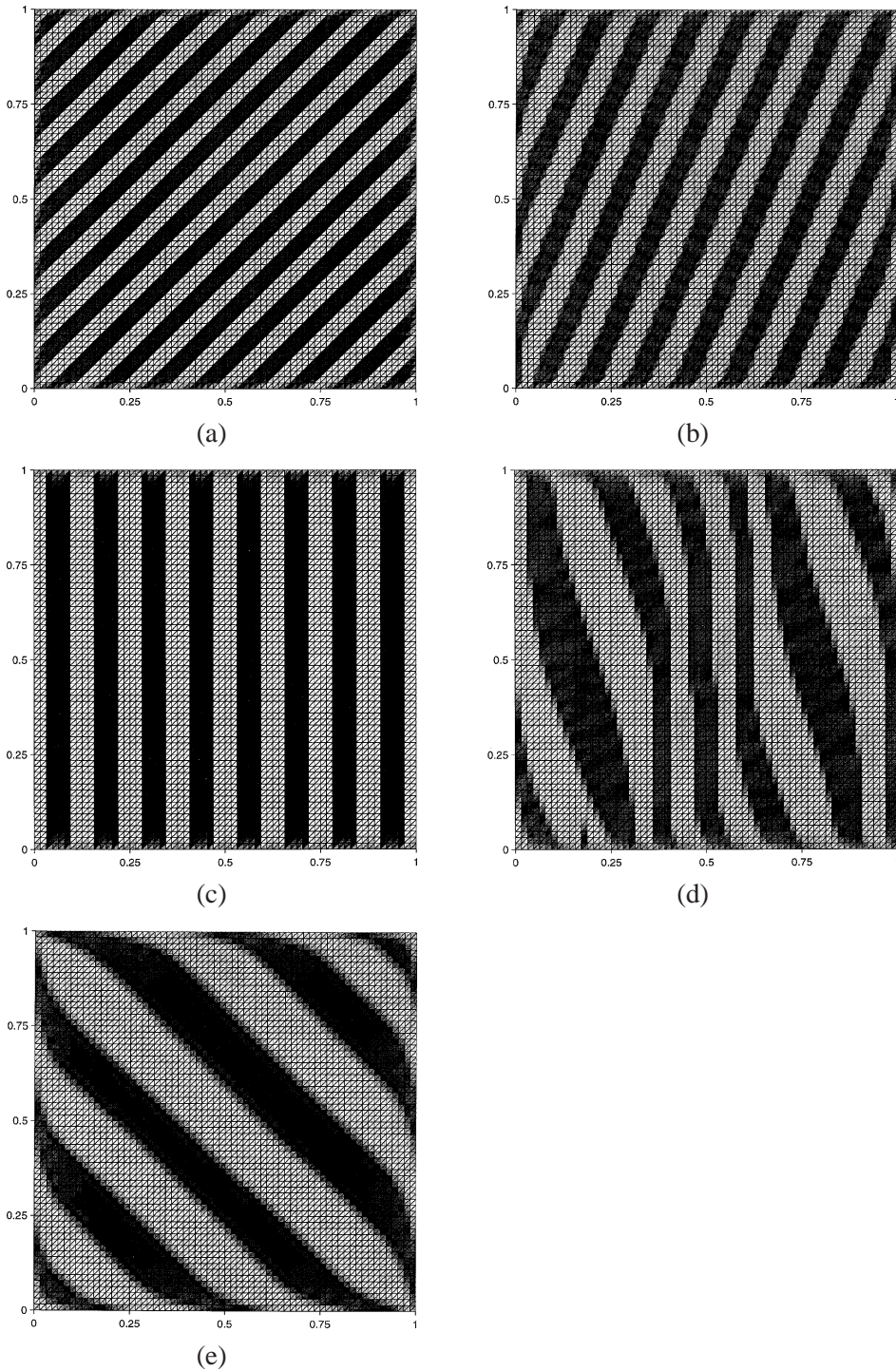


Fig. 1. Prototype problem, computed volume fractions for the conforming element with  $\alpha_2 = 1000$  using  $h = \frac{1}{64}$ , (a)  $\gamma = -45^\circ$ , (b)  $\gamma = -22.5^\circ$ , (c)  $\gamma = 0^\circ$ , (d)  $\gamma = 22.5^\circ$ , (e)  $\gamma = 45^\circ$ .

As a unique feature of using a one-dimensional prototype problem, it is possible to plot also the deformation itself in Fig. 4(a); the deformation for the larger  $h = \frac{1}{16}$  is shown for visibility. It can be seen that the boundary conditions are indeed satisfied and that the transition to the laminate structure in the interior is limited to a small layer close to the boundary. Thus, the penalization technique is seen to work effectively, and the contribution from the boundary to the total energy is (much) less than 10%. That is, practically all error in the conforming finite element method with exact boundary conditions results from the bulk term in the energy functional. This motivates the relaxation of the enforcement of the boundary conditions by choosing smaller values for  $\alpha_2$ . As is well-understood theoretically, this results in improved convergence for aligned meshes, whereas no improvement is visible in the non-aligned cases; see Tables 2(b), 3(b), 4(b), and 5(b).

## 2.2. The classical non-conforming finite element

This element has been proposed for the simulation of microstructures in order to increase the flexibility of the finite element approximation, when adjusting to non-aligned meshes; see [9,12,16,20]. All cases in Fig. 2 show that the increased flexibility allows for a better representation of the laminates, while the boundary conditions are still satisfied exactly, see Fig. 4(b). However, Table 2(c) shows that the convergence behavior has not improved over the conforming element. It is observed that the bulk term of the energy still accounts for more than 90% of the energy, that is the mesh pollution effect on the minimizer is still present.

As in the conforming case, the enforcement of the boundary conditions in the penalty formulation is further relaxed by decreasing the value of  $\alpha_2$ . As Tables 2(d), 3(d), 4(d), and 5(d) show, any improvements are concentrated on the aligned cases of angles  $\gamma = -45^\circ$  and  $\gamma = 0^\circ$ , as for the conforming element. It has to be concluded that the classical non-conforming element possesses more flexibility to represent the laminates (see the figures), but it does not decrease the interpolation error independently of the mesh alignment (see the tables), thus validating the theoretical result (6) in general.

## 2.3. The discontinuous finite element

Fig. 3 shows the computed volume fraction for the discontinuous element. The laminates are wider than for the classical elements due to the scaling used in the scaled energy functional (7). As the figure and Table 2(e) show, the results as well as the convergence behavior are independent of the mesh alignment. We can observe nearly quadratic convergence rates in most entries, in agreement with the theoretical prediction in Table 1.

Tables 3(e) and 4(e) exhibit slightly better convergence rates than predicted in Table 1. On the one hand, the absolute values for the error in the deformation in Table 3(e) are slightly higher than for the previous elements due to the wider laminates. On the other hand, the values for the error in the deformation gradient in laminate direction in Table 4(e) are significantly smaller than before, which are well-resolved. Finally, Table 5(e) shows that the volume fraction  $\mu(\omega_\rho^i(u_h))/\mu(\omega)$  is computed without error in many instances for general meshes, an observation that is in contrast with the previous methods.

The difference in the energy between aligned and non-aligned cases is made up nearly solely by contributions from the jump terms with coefficients  $\alpha_{11}$  and  $\alpha_{12}$ , which are very small in the aligned cases. However, if the resolution is sufficiently good ( $h \leq \frac{1}{32}$ ), the bulk term in the energy functional contributes

at most 5% to the total energy. This demonstrates that the discontinuous finite element method is capable of resolving the simple laminate structure on general meshes, since the interpolation error is uniformly small.

### 3. Example 2: Tartar's example with non-zero energy

This section shows the increased flexibility of the discontinuous finite element method in another test example due to Tartar, see [22], involving a more complicated microstructure. Numerical studies on this problem for convexified energies or generalized formulations have been performed in [22] and [4,5], respectively.

We consider the minimization of the following energy, for  $\Omega = (0, 1) \times (0, 1)$ ,

$$\tilde{\mathcal{E}}(v) = \int_{\Omega} (v_x^2 - 1)^2 + v_y^2 \, dx + \int_{\Omega} \left[ -\frac{3}{128} \left(x - \frac{1}{2}\right)^5 - \frac{1}{3} \left(x - \frac{1}{2}\right)^3 - v \right]^2 \, dx. \quad (12)$$

It is known that the minimum of the relaxed problem is given by

$$u(x, y) = \begin{cases} -\frac{3}{128} \left(x - \frac{1}{2}\right)^5 - \frac{1}{3} \left(x - \frac{1}{2}\right)^3 & \text{for } 0 \leq x \leq \frac{1}{2}, \\ \frac{1}{24} \left(x - \frac{1}{2}\right)^3 + \left(x - \frac{1}{2}\right) & \text{for } \frac{1}{2} < x \leq 1. \end{cases} \quad (13)$$

The minimum energy [23] is given by a positive value, i.e.,  $\inf_{v \in \tilde{\mathcal{A}}} \tilde{\mathcal{E}}(v) = \frac{1409}{30000}$ , for  $\tilde{\mathcal{A}} = \{v \in W_g^{1,4}(\Omega), g = u|_{\partial\Omega}\}$ , and minimizing sequences exhibit spatial oscillations, i.e., microstructure, on the domain  $m = (0, \frac{1}{2}) \times (0, 1)$ .

The conforming and the discontinuous finite element methods were applied to this problem in order to study the impact of general triangulations and given boundary data on computed minimizers. To this end, the energy functional (12) is 'rotated' in the same way as in (10) for the energy functional in (9). For a rotation of  $\gamma = +22.5^\circ$ , the solution deformation has the form as shown in Fig. 5 with the microstructure in the front part of the graphs.

The results for the computed volume fractions are presented in Figs. 6 and 7 for the conforming and the discontinuous element, respectively. There is again significant pollution of the laminate microstructure on parts of the domain for the conforming method in Fig. 6. The discontinuous method produces the volume fractions in Fig. 7 with crisp laminates in the appropriate part of the domain, for all rotation angles  $\gamma$ .

### 4. Example 3: Two-dimensional modeling for simple laminates

This example deals with a physically relevant situation modeling orthorhombic to monoclinic transformation [19]. Its two-dimensional deformation  $v : \Omega \rightarrow \mathbb{R}^2$  minimizes the energy

$$\mathcal{E}(v) = \int_{\Omega} \phi(\nabla v(x)) \, dx \quad (14)$$

with energy density

$$\phi(F) = \kappa_1 (C_{11} - (1 + \eta^2))^2 + \kappa_2 (C_{22} - 1)^2 + \kappa_3 (C_{12}^2 - \eta^2)^2, \quad (15)$$

where  $C = F^T F$  is the Cauchy–Green strain tensor and  $\eta$ ,  $\kappa_1$ ,  $\kappa_2$ , and  $\kappa_3$  are positive constants. Its energetically favored deformation gradients are

$$F_1 = \begin{pmatrix} 1 & 0 \\ -\eta & 1 \end{pmatrix} \quad \text{and} \quad F_2 = \begin{pmatrix} 1 & 0 \\ +\eta & 1 \end{pmatrix}. \quad (16)$$

The boundary condition is given by the average gradient as

$$v(x) = [(1 - \lambda)F_1 + \lambda F_2]x \quad \text{for all } x \in \partial\Omega; \quad (17)$$

it is chosen  $\lambda = \frac{1}{2}$  in the simulations. The constants in the energy density are chosen as  $\eta = 0.1$  and  $\kappa_1 = \kappa_2 = \kappa_3 = 1$ .

The plots in the following show the observed distances of the deformation gradient  $F$  on each element from the favored gradient matrix  $F_1$ ; more formally, each element is colored representing a scale from 0 to 1 according to the function [19]

$$\psi(F) = \frac{\|F^T F - F_1^T F_1\|_F^2}{\|F^T F - F_1^T F_1\|_F^2 + \|F^T F - F_2^T F_2\|_F^2}. \quad (18)$$

This leads to plots that visualize both the direction of the laminates as well as the observed volume fractions.

Results for the conforming element are shown in Fig. 8. The initial guess for the deformation was chosen as accurately as the discretization on each grid allows for the continuous deformation. Despite the good initial guess, the finite element discretization could not maintain the structure of the deformation while minimizing the energy in the misaligned cases in Fig. 8(d), similar to results in [19]. Even worse, the direction of the laminates in Fig. 8(e) follows the *numerical* grid, entirely contradicting the physics of the problem; this effect has also been reported in [21, Fig. 13].

Fig. 9 summarizes the results for the discontinuous element. This finite element is able to discretize the physical laminates equally well for all angles  $\gamma$ . The initial guesses for the results were also chosen close to the solution. It is a known problem of direct minimization that the gradient based minimizers risk getting stuck in local minima for non-convex problems, and this is exhibited by poor convergence behavior and strong dependence on the initial guess. However, it is demonstrated that the finite element is able to resolve the physical structure on the given uniform mesh.

Finally, we notice that in the well-aligned cases, the conforming element is able to find an energy minimum corresponding to narrower laminates than the discontinuous element. This demonstrates of course that the latter element got stuck in some local minimum. However, for the approximation of the most important quantities like the volume fraction in some relevant subset of the domain, it is more important to be able to guarantee that the relevant physics (direction of laminates and the proportion of phases) are represented correctly; this is not satisfied by the conforming element in general, and the narrower laminates do not provide any benefit.

## 5. Conclusions

Results for detailed case studies for relevant prototype problems for the simulation of crystalline microstructure have been presented for three finite elements: conforming, classical non-conforming, and discontinuous finite elements. The quality of both the conforming and the classical non-conforming elements are seen to depend on the alignment of the numerical grid with the physical laminates,

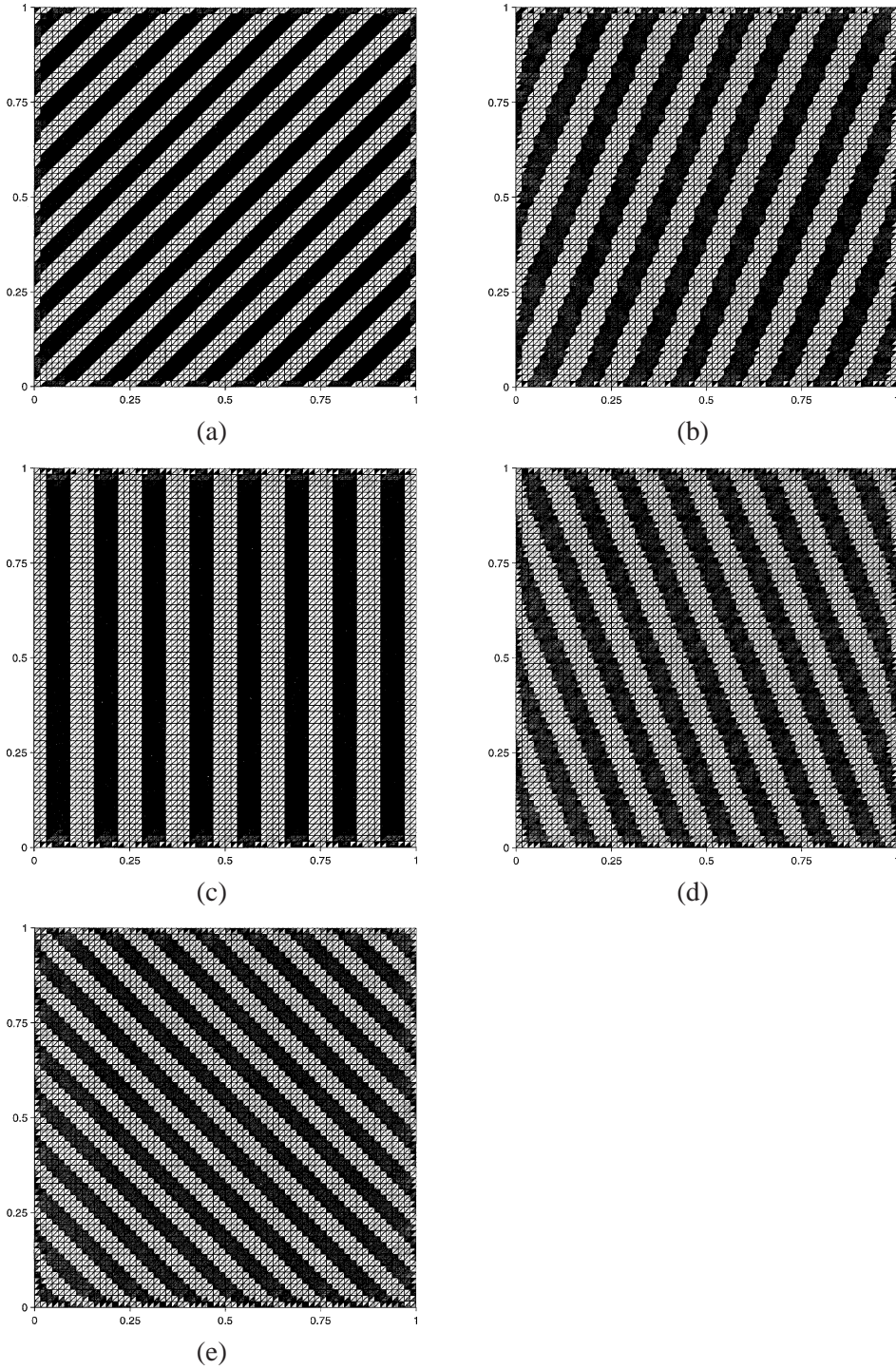


Fig. 2. Prototype problem, computed volume fractions for the non-conforming element with  $\alpha_2 = 1000$  using  $h = \frac{1}{64}$ , (a)  $\gamma = -45^\circ$ , (b)  $\gamma = -22.5^\circ$ , (c)  $\gamma = 0^\circ$ , (d)  $\gamma = 22.5^\circ$ , (e)  $\gamma = 45^\circ$ .

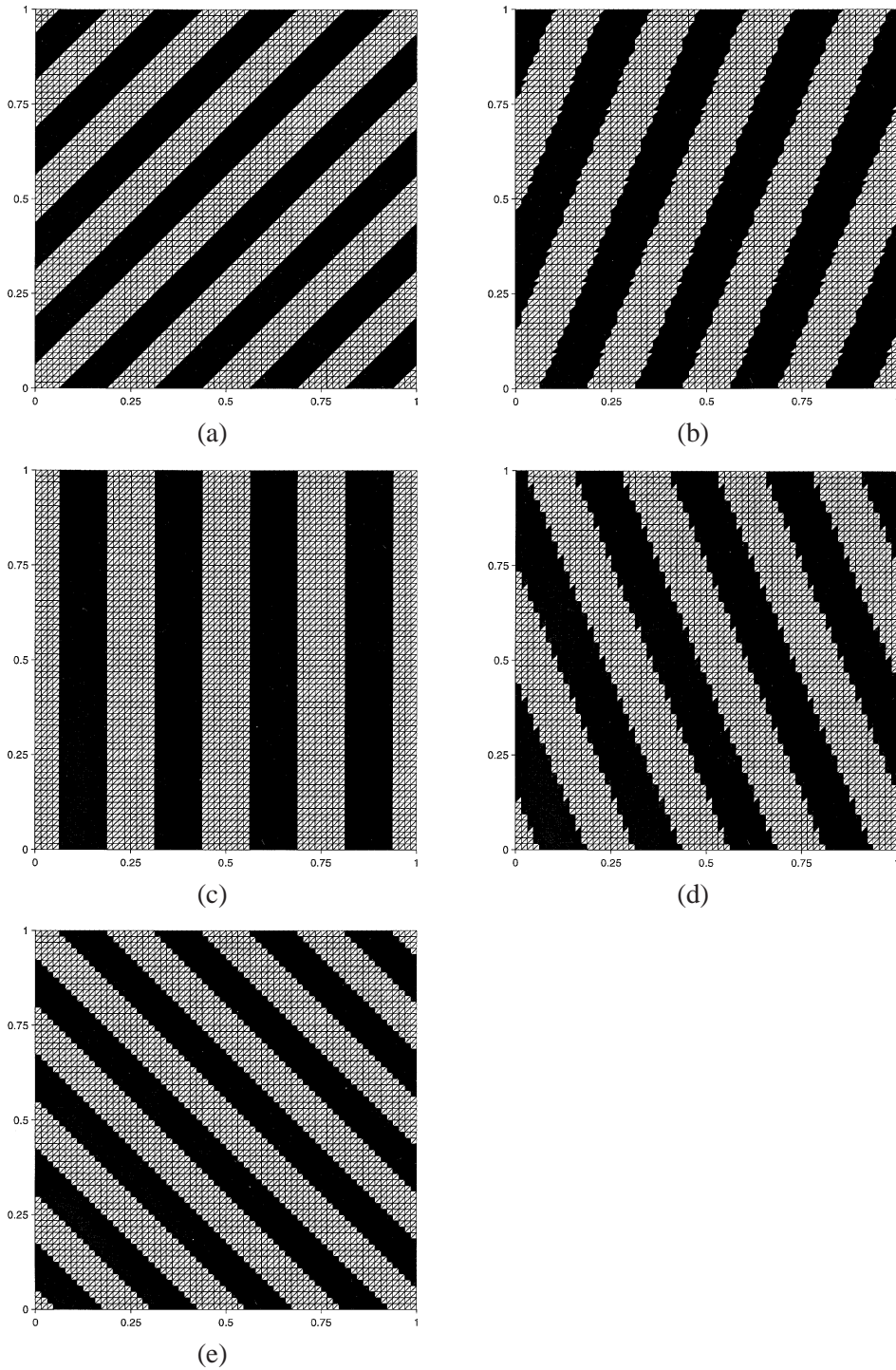


Fig. 3. Prototype problem, computed volume fractions for the discontinuous element using  $h = \frac{1}{64}$ , (a)  $\gamma = -45^\circ$ , (b)  $\gamma = -22.5^\circ$ , (c)  $\gamma = 0^\circ$ , (d)  $\gamma = 22.5^\circ$ , (e)  $\gamma = 45^\circ$ .

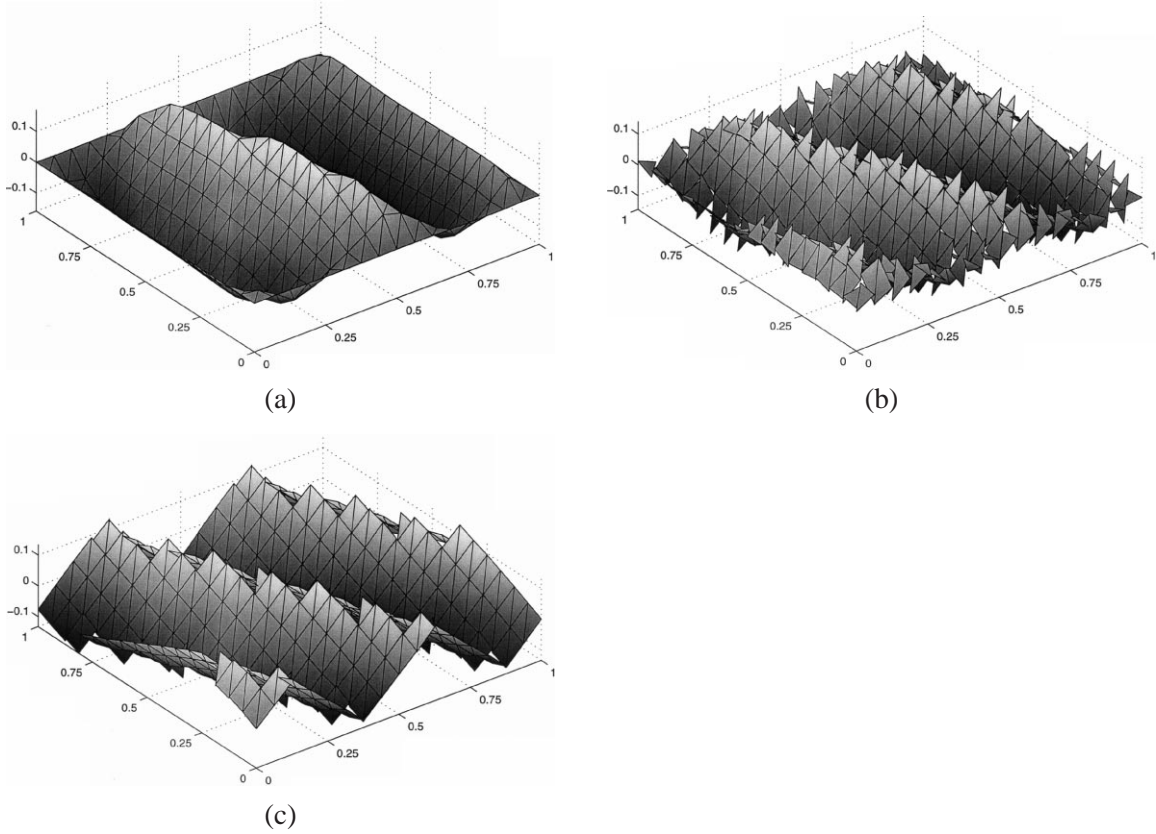


Fig. 4. Prototype problem, computed deformation for  $\gamma = 22.5^\circ$  using  $h = \frac{1}{16}$ , (a) for the conforming element with  $\alpha_2 = 1000$ , (b) for the non-conforming element with  $\alpha_2 = 1000$ , (c) for the discontinuous element.

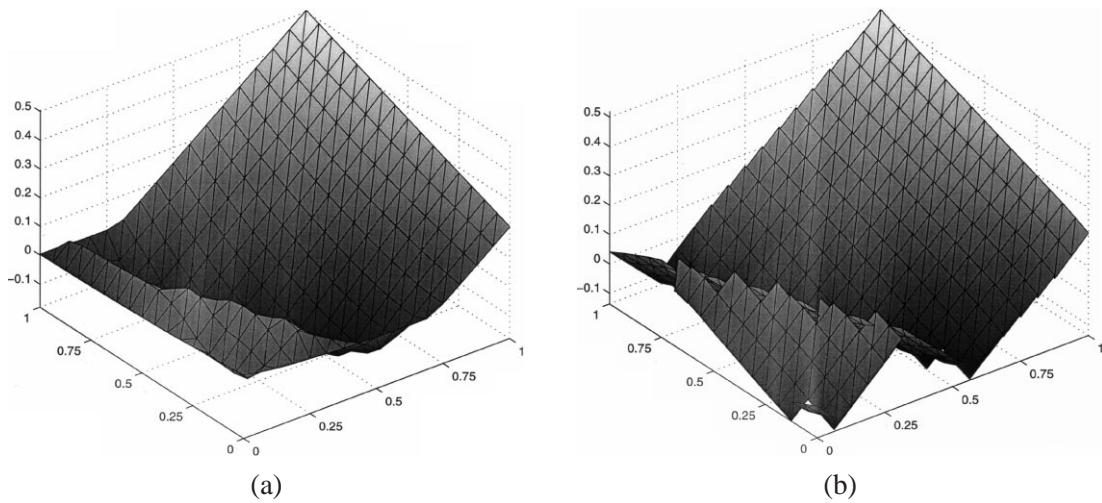


Fig. 5. Tartar's example, computed deformation for  $\gamma = 22.5^\circ$  using  $h = \frac{1}{16}$ , (a) for the conforming element with  $\alpha_2 = 1000$ , (b) for the discontinuous element.

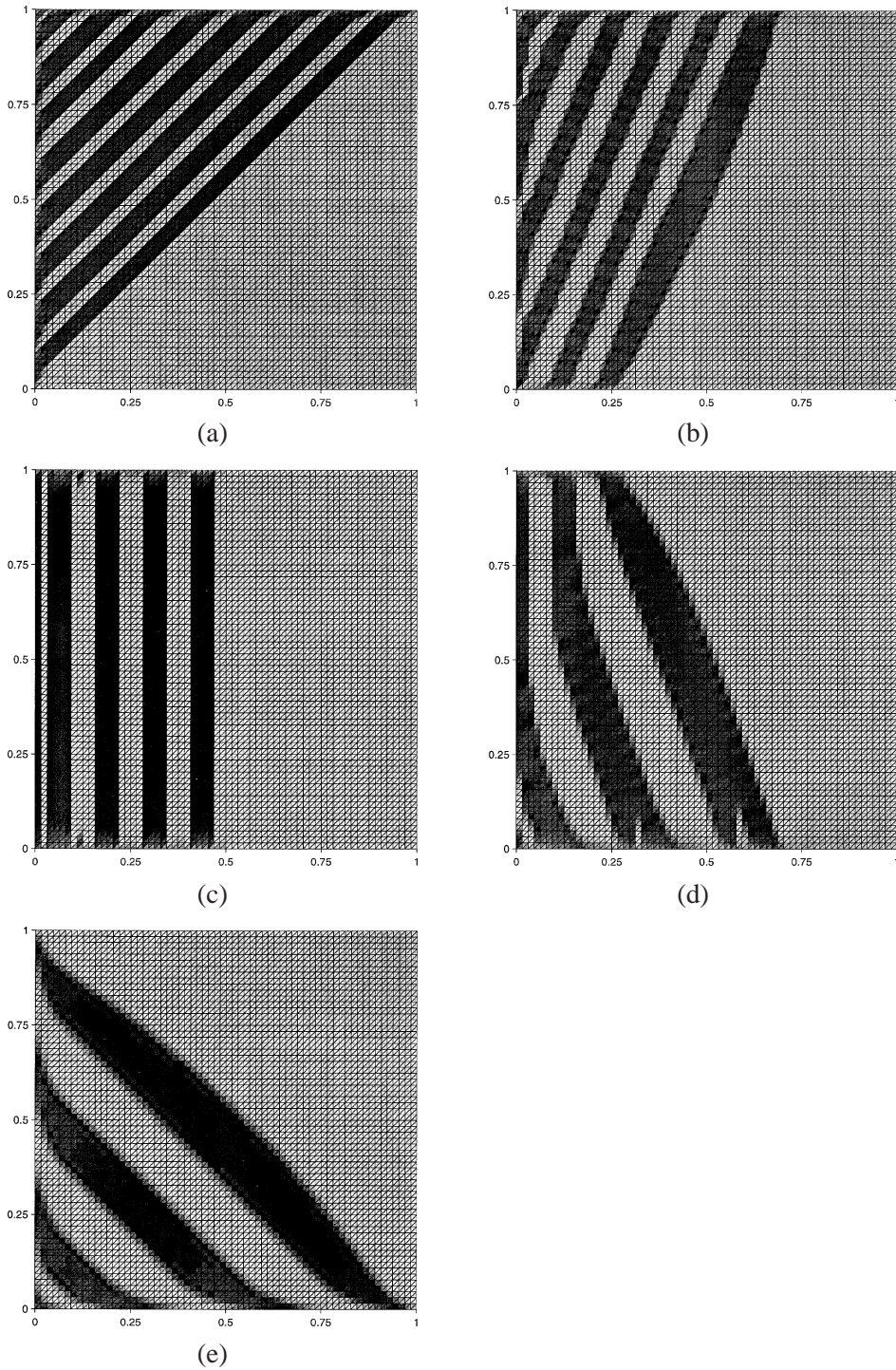


Fig. 6. Tartar's example, computed volume fractions for the conforming element with  $\alpha_2 = 1000$  using  $h = \frac{1}{64}$ , (a)  $\gamma = -45^\circ$ , (b)  $\gamma = -22.5^\circ$ , (c)  $\gamma = 0^\circ$ , (d)  $\gamma = 22.5^\circ$ , (e)  $\gamma = 45^\circ$ .

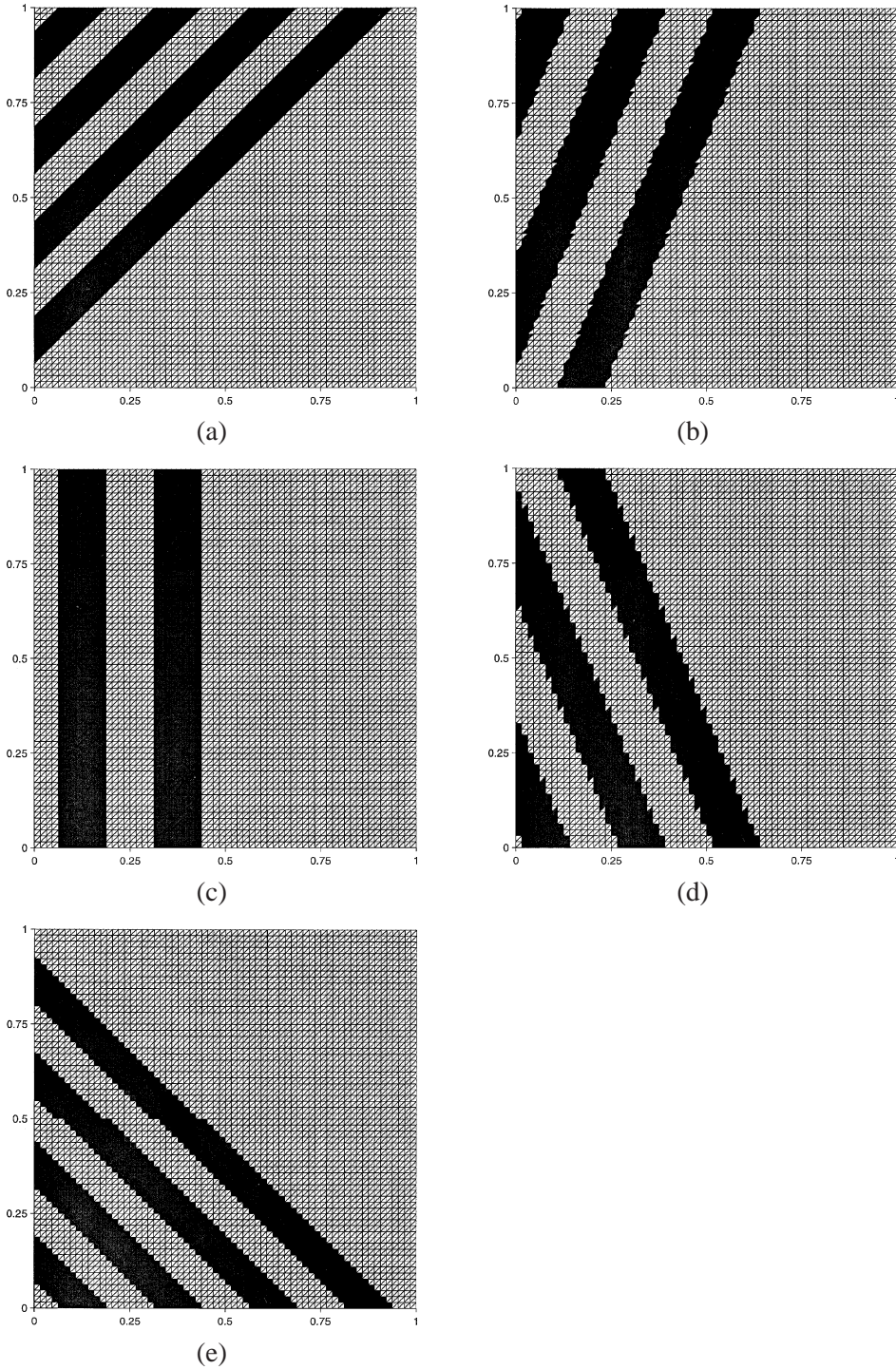


Fig. 7. Tartar's example, computed volume fractions for the discontinuous element using  $h = \frac{1}{64}$ , (a)  $\gamma = -45^\circ$ , (b)  $\gamma = -22.5^\circ$ , (c)  $\gamma = 0^\circ$ , (d)  $\gamma = 22.5^\circ$ , (e)  $\gamma = 45^\circ$ .

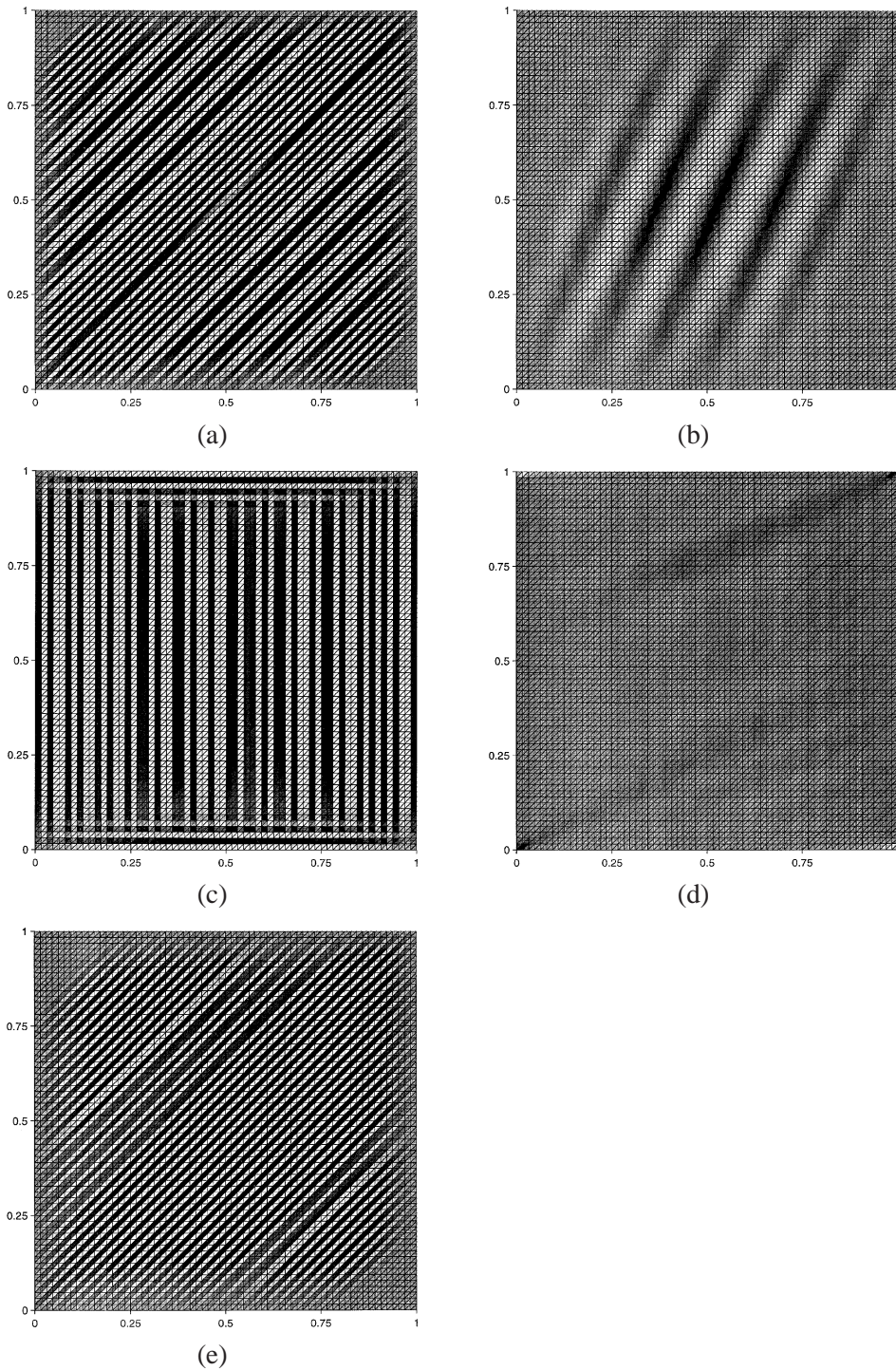


Fig. 8. Two-dimensional model, computed volume fractions for the conforming element with  $\alpha_2 = 1000$  using  $h = \frac{1}{64}$ , (a)  $\gamma = -45^\circ$ , (b)  $\gamma = -22.5^\circ$ , (c)  $\gamma = 0^\circ$ , (d)  $\gamma = 22.5^\circ$ , (e)  $\gamma = 45^\circ$ .

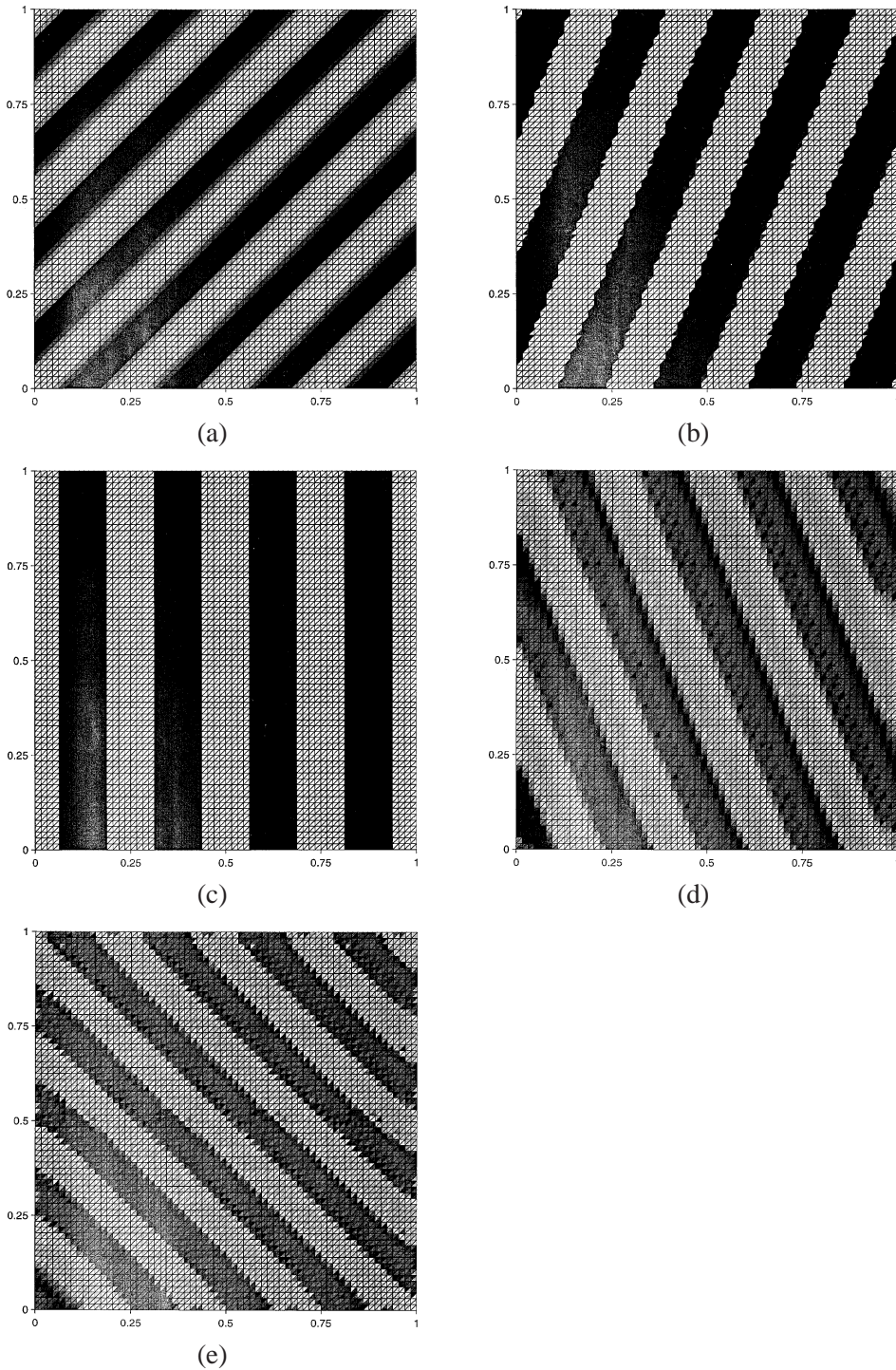


Fig. 9. Two-dimensional model, computed volume fractions for the discontinuous element using  $h = \frac{1}{64}$ , (a)  $\gamma = -45^\circ$ , (b)  $\gamma = -22.5^\circ$ , (c)  $\gamma = 0^\circ$ , (d)  $\gamma = 22.5^\circ$ , (e)  $\gamma = 45^\circ$ .

with decreasing quality on general triangulations. The relaxation of the enforcement of the boundary conditions alone in the case of the classical elements did not improve their convergence behavior. In contrast, the results of the case study for the discontinuous element show optimal convergence behavior on general meshes, independent of the mesh alignment. All three elements studied in this paper represent the macroscopic deformation quite well, but only the discontinuous element represents the crucial microscopic quantities like the deformation gradient in laminate direction and the coefficient of the corresponding Young measure adequately. Also for the more complex microstructures in Sections 3 and 4, the discontinuous element shows superior performance compared to the classical elements. These computational results are in agreement with analytic results contained in [11].

## Acknowledgements

The first author would like to acknowledge partial support by a summer grant from the University of Maryland, Baltimore County, and from the National Science Foundation under grant DMS-9805547. The second author gratefully acknowledges support through a scholarship from the Deutsche Forschungsgemeinschaft.

## References

- [1] J. Ball, R. James, Fine phase mixtures as minimizers of energy, *Arch. Rat. Mech. Anal.* 100 (1987) 13–52.
- [2] J. Ball, R. James, Proposed experimental tests of a theory of fine microstructure and the two-well problem, *Phil. Trans. Roy. Soc. London Ser. A* 338 (1992) 389–450.
- [3] H. Blum, J. Harig, S. Müller, S. Turek, FEAT2D: Finite element analysis tools. User manual. Release 1.3, Technical Report, Universität Heidelberg, 1992.
- [4] C. Carstensen, P. Plecháč, Numerical solution of the scalar double-well problem allowing microstructure, *Math. Comp.* 66 (1997) 997–1026.
- [5] C. Carstensen, P. Plecháč, Adaptive algorithms for scalar non-convex variational problems, *Appl. Numer. Math.* 26 (1998) 203–216.
- [6] C. Carstensen, T. Roubíček, Numerical approximation of Young measures in non-convex variational problems, Technical Report 97-18, Universität Kiel, 1997.
- [7] M. Chipot, C. Collins, D. Kinderlehrer, Numerical analysis of oscillations in multiple well problems, *Numer. Math.* 70 (1995) 259–282.
- [8] C. Collins, Computation and analysis of twinning in crystalline solids, Ph.D. thesis, University of Minnesota, 1990.
- [9] C. Collins, Comparison of computational results for twinning in the two-well problem, in: C. Rogers, G. Wallace (Eds.), *Proceedings of the 2nd International Conference on Intelligent Materials*, Technomic, 1994, pp. 391–401.
- [10] B. Dacorogna, *Direct Methods in the Calculus of Variations*, Springer, 1989.
- [11] M.K. Gobbert, A. Prohl, A discontinuous finite element method for solving a multiwell problem, *SIAM J. Numer. Anal.* 37 (2000) 246–268.
- [12] P. Gremaud, Numerical analysis of a nonconvex variational problem related to solid-solid phase transitions, *SIAM J. Numer. Anal.* 31 (1994) 111–127.
- [13] P. Klouček, M. Luskin, The computation of the dynamics of martensitic microstructure, *Continuum Mech. Thermodyn.* 6 (1994) 209–240.

- [14] M. Kružík, Numerical approach to double well problems, *SIAM J. Numer. Anal.* 35 (1998) 1833–1849.
- [15] B. Li, M. Luskin, Finite element analysis of microstructure for the cubic to tetragonal transformation, *SIAM J. Numer. Anal.* 35 (1998) 376–392.
- [16] B. Li, M. Luskin, Nonconforming finite element approximation of crystalline microstructure, *Math. Comp.* 67 (1998) 917–946.
- [17] D.G. Luenberger, *Linear and Nonlinear Programming*, 2nd Edition, Addison-Wesley, Reading, MA, 1989.
- [18] M. Luskin, Approximation of a laminated microstructure for a rotationally invariant, double well energy density, *Numer. Math.* 75 (1996) 205–221.
- [19] M. Luskin, On the computation of crystalline microstructure, *Acta Numer.* 5 (1996) 191–257.
- [20] L. Ma, N.J. Walkington, On algorithms for nonconvex optimization in the calculus of variations, *SIAM J. Numer. Anal.* 32 (1995) 900–923.
- [21] R.A. Nicolaides, N. Walkington, H. Wang, Numerical methods for a nonconvex optimization problem modeling martensitic microstructure, *SIAM J. Sci. Comput.* 18 (1997) 1122–1141.
- [22] R.A. Nicolaides, N.J. Walkington, Strong convergence of numerical solutions to degenerate variational problems, *Math. Comp.* 64 (1995) 117–127.
- [23] P. Pedregal, *Parameterized Measures and Variational Principles*, Birkhäuser, Basel, 1997.
- [24] T. Roubíček, *Relaxation in Optimization Theory and Variational Calculus*, Walter de Gruyter, Berlin, New York, 1997.